How to cite: *Angew. Chem. Int. Ed.* **2022,** *61,* e202200206
International Edition: doi.org/10.1002/anie.202200206
German Edition: doi.org/10.1002/ange.202200206

Analytical Methods

Ultrafast Electrothermal Flow-Enhanced Magneto Biosensor for Highly Sensitive Protein Detection in Whole Blood

*Jiran Li and Peter B. Lillehoj**

Abstract: Current diagnostic tests for sensitive protein detection rely on immunological techniques, such as ELISA, which require sample purification, multiple washing steps and lengthy incubation, hindering their use for rapid testing. Here, we report a simple electrothermal flow-enhanced biosensor for ultrafast, high sensitivity measurements of protein biomarkers in whole blood. Magnetic nanobeads dually-labeled with a detection antibody and enzyme reporter are used to form immunocomplexes with the target protein, which are readily transported to the sensor via magnetic concentration. The incorporation of electrothermal flows enhances immunocomplex formation, allowing for rapid and sensitive detection without requiring blood purification or lengthy incubation. Proof of concept was carried out using *Plasmodium falciparum* histidine-rich protein 2 (*Pf*HRP2), a malaria parasite biomarker, which could be detected at concentrations as low as 5.7 pg mL^{-1} (95 fM) in whole blood in 7 min. The speed, sensitivity and simplicity of this device make it attractive for rapid diagnostic testing.

Introduction

Diagnostic tests based on the detection and quantification of protein biomarkers are used for several important clinical applications, such as medical screening,[1,2] disease diagnosis[3–5] and monitoring response to treatment.[6–8] Currently, the most common laboratory technique for sensitive, quantitative detection of protein biomarkers in biological fluids is enzyme-linked immunosorbent assay (ELISA), which is considered the clinical gold standard.[9] However, ELISA requires bulky equipment for sample purification (i.e., centrifugation) and involves multiple washing steps and lengthy incubation (≈1.5–3 h in total), making it labor-intensive, time-consuming and limited to laboratory settings.[10,11] Prior efforts have been carried out to achieve high sensitivity detection of protein biomarkers in whole blood without the need for sample purification. Joh et al. developed an inkjet-printed fluorescence immunoassay that could detect IL-6 in chicken blood with a lower limit of detection (LOD) of 10.9 pg mL^{-1}.[12] Zupančič et al. reported an electrochemical immunoassay for detecting sepsis biomarkers, which exhibited a lower LOD of 24.7 pg mL^{-1} in 50 % whole blood.[13] Minopoli et al. demonstrated the detection of *Plasmodium falciparum* lactate dehydrogenase (*Pf*LDH) in diluted (1:100) whole blood using a fluorescence immunosensor with a lower LOD of 0.6 pg mL^{-1}.[14] While these techniques are capable of detecting proteins in whole blood with high sensitivity, they involve multiple washing steps and lengthy (50 min–4 h) incubation, hindering their use for applications requiring fast turnaround times, such as on-site testing or point-of-care testing. The ability to achieve rapid protein detection with high analytical sensitivity in whole blood is hampered by inefficient mass transport and slow protein binding kinetics in the complex liquid matrix.[15] Various techniques have been demonstrated to enhance mass transport and kinetics in surface binding assays, such as the use of microfluidic flows to confine the sample to the sensor surface[16] or continuously refresh the sensor with fresh analyte.[17] While these methods are capable of increasing the analytical sensitivity and reducing the assay time, they require complicated fluidic systems or result in increased sample/reagent consumption. Alternatively, direct current (DC) electrokinetics[18] or alternating current (AC) electrokinetics[19–21] has been shown to be an effective technique for manipulating and separating biomolecules in small volume samples. However, electrokinetics typically requires high operating voltages, which can cause electrolysis, and its performance is highly dependent on the fluid properties (e.g., conductivity, viscosity).[22] For these reasons, electrokinetic-based fluid manipulation is less effective for complex biological matrices, such as whole blood or minimally diluted blood.

AC electrothermal flow (ACEF) is an alternative technique for generating microflows in small volume samples where an AC electrical field is applied to planar electrodes, resulting in non-uniform Joule heating. This localized Joule heating gives rise to gradients in permittivity and conductivity of the fluid, which generates thermally driven fluid forces that leads to swirling flows.[23] In contrast to electrokinetic-driven flow, ACEF is compatible with a broader range of biological fluids and can offer greater control over fluid motion. Computational and experimental studies by Lu et al. revealed the essential role of buoyancy force in long-range ACEF motion in microchannels.[24]

[*] J. Li, Prof. P. B. Lillehoj
Department of Mechanical Engineering, Rice University
Houston, TX 77005 (USA)
E-mail: lillehoj@rice.edu
Prof. P. B. Lillehoj
Department of Bioengineering, Rice University
Houston, TX 77030 (USA)

Numerical studies by Sigurdson et al. further showed that electrothermally induced micro-stirring inside microchannels can improve antigen-antibody binding for flow-through assays.[25] ACEF has also been shown to enhance the performance of electrical biosensors for the detection of nucleic acids[26] and proteins;[27] however, these approaches involve multiple incubation steps requiring >30 min and are unable to achieve single pg mL^{-1} sensitivity in whole blood.

Magnetic beads are widely used in immunoassays for biomolecular separation and enrichment.[28,29] Prior reports have demonstrated electrochemical sensors employing magnetic beads for rapid, quantitative biomolecular detection.[30–32] However, these platforms require multiple sample processing steps and were limited to purified serum samples. In our previous work, we showed that the use of magnetic nanobeads combined with immunomagnetic enrichment could generate an amplified electrochemical signal, enabling high sensitivity electrochemical detection.[33] However, like many immunosensors, this approach still involved lengthy (≥ 1 h) incubation and required purified serum samples for highly sensitive measurements. To address these limitations, we have developed a rapid, highly sensitive magneto-immunosensor that employs ACEF mixing for accelerated mass transport and immunocomplex formation. This immunosensor utilizes dually-labeled magnetic nanobeads (DMBs) that are coated with a detection antibody and enzyme reporter to form immunocomplexes with the target protein, allowing for simplified immunomagnetic enrichment and increased signal amplification. We show that ACEF mixing enhances biomolecular transport and promotes immunocomplex formation, enabling high sensitivity detection at single pg mL^{-1} (<100 fM) levels without requiring sample purification or lengthy incubation. Proof of concept is demonstrated by detecting *Plasmodium falciparum* histidine-rich protein 2 (*Pf*HRP2), a biomarker for *P. falciparum*, which accounts for $>90\,\%$ of global fatalities due to malaria infection.[34] Measurements of *Pf*HRP2 in clinical blood samples obtained from malaria-infected individuals reveal that this immunosensor offers greater diagnostic accuracy than a commercial *Pf*HRP2 ELISA kit, while being much faster and simpler to perform.

Results and Discussion

Design of the ACEF-Enhanced Electrochemical Magneto-Immunosensor

Many surface binding assays rely on diffusion-based mass transport to bring the relevant biomolecules (e.g., target analyte, detection antibody, reporter molecule) close to the reactive surface. For microwell immunoassays, such as ELISA, the distance that biomolecules need to travel to move from the bulk solution to the capture antibody-immobilized surface is several orders of magnitude larger than their diffusion length, necessitating long (≈ 1 h) incubation periods for mass transport.[35] Methods to enhance mass transport in microwell immunoassays, such as performing incubation at elevated temperatures and/or incorporating agitation, have been shown to offer moderate improvements in the analytical sensitivity and reductions in the assay time.[36] However, incorporating these methods with this magneto-immunosensor resulted in a negligible improvement in the sensor performance (Figure S2C). Therefore, we employed an alternative technique to accelerate mass transport and enhance immunocomplex formation through the generation of electrothermally driven flows in the sample.

A schematic illustrating the design and working principle of the ACEF-enhanced magneto-immunosensor is shown in Figure 1. The screen-printed gold electrode (SPGE) sensor consists of an Au working electrode (WE), Au counter electrode (CE) and Ag/AgCl reference electrode (RE). The electrodes are situated within a 4 mm diameter, 100 μm thick polyethylene terephthalate (PET) well, which confines the blood droplet on the sensor and ensures that the electrodes are fully immersed during the measurement (Figure S3). The WE is coated with anti-*Pf*HRP2 IgM, which is used as the capture antibody. To initiate the measurement, the blood sample is mixed with DMBs and dispensed onto the sensor. DMBs are coated with horseradish peroxidase (HRP) and HRP-conjugated anti-*Pf*HRP2 IgG, which is used as the detection antibody. If the target antigen is present in the sample, it binds to the DMB, forming an antigen-DMB immunocomplex. An AC potential is applied between the WE and CE for 5 min for ACEF mixing, which enhances mass transport and promotes the formation of the antigen-DMB immunocomplexes (Figure 1A). After 4 min of ACEF mixing, a magnet is placed under the sensor, which generates a localized magnetic field, causing the antigen-DMB immunocomplexes to rapidly migrate to the sensor surface where they subsequently bind to the capture antibody-immobilized WE (Figure 1B). In the presence of TMB substrate, HRP immobilized on the DMB catalyzes the reduction of H_2O_2 coupled to TMB oxidation. The oxidized TMB is reduced upon the application of a bias potential, generating an amperometric current that is proportional to the concentration of target antigen attached to the sensor surface (Figure 1C). The entire detection process is completed in 7 min. If the sample does not contain the target antigen, then the DMBs are washed away from the sensor surface and a negligible electrochemical signal is generated upon the application of a bias potential in the presence of TMB substrate.

To verify that the amperometric signals generated by the immunosensor are due to the binding of antigen-DMB immunocomplexes to the capture antibody-immobilized WE, measurements of $5\times$ diluted blood spiked with *Pf*HRP2 at 0 ng mL^{-1} and 1 ng mL^{-1} were performed using sensors coated with anti-*Pf*HRP2 IgM capture antibody and sensors without capture antibody. As shown in Figure S4, negligible ΔI values, which represent the difference in the amperometric signal between the positive (1 ng mL^{-1}) and negative (0 ng mL^{-1}) controls, were generated by the sensors without capture antibody. In contrast, significantly large ΔI values (≈ 990 nA) were generated by the capture antibody-immobilized sensors, demonstrating that the amperometric signals generated during the electrochemical reaction are due to the

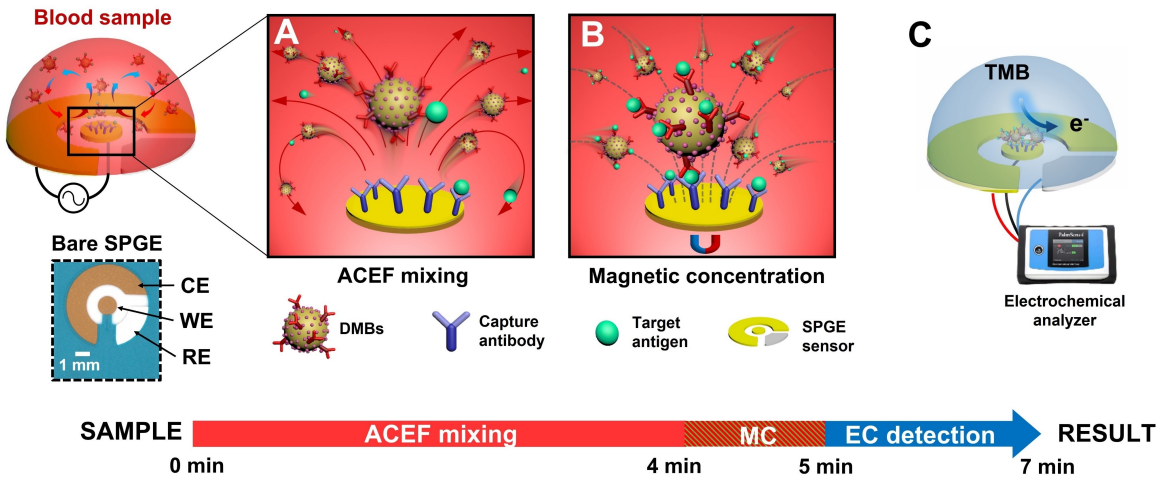

Figure 1. Design and working principle of the ACEF-enhanced magneto-immunosensor. A) Schematic illustration of the blood sample premixed with dually-labeled magnetic nanobeads (DMBs) on the screen-printed gold electrode (SPGE) sensor. Upon application of an AC potential between the working electrode (WE) and counter electrode (CE), swirling microflows are generated within the droplet due to electrothermally induced forces, enhancing the transport of proteins and DMBs in the sample and promoting the formation of antigen-DMB immunocomplexes. B) Schematic depicting the magnetic concentration (MC) of antigen-DMB immunocomplexes on the capture antibody-immobilized sensor surface, which is achieved by placing the SPGE sensor on a permanent magnet. C) Schematic illustration of the electrochemical (EC) sensing scheme after the SPGE sensor has been rinsed and loaded with TMB substrate. Horseradish peroxidase immobilized on the DMBs catalyzes the reduction of H_2O_2 coupled to TMB oxidation. The oxidized TMB is reduced upon the application of a bias potential between the WE and CE, which generates an amperometric current that is proportional to the concentration of target antigen attached to the sensor surface.

formation of a sandwich structure constituting the binding of antigen-DMB immunocomplexes to the capture antibody-immobilized sensor and not due to non-specific attachment of antigen-DMB immunocomplexes on the sensor surface.

The large amount of HRP on each DMB (≈470 active HRP molecules per nanobead, details are in the Supporting Information) results in the generation of an amplified amperometric signal during the electrochemical reaction, enabling the detection of very low protein concentrations. We investigated the improvement in signal amplification using DMBs by performing measurements of 5× diluted blood spiked with *Pf*HRP2 at 0 ng mL^{-1} and 1 ng mL^{-1} using DMBs or magnetic nanobeads labeled with HRP-conjugated anti-*Pf*HRP2 IgG only. As shown in Figure S5, ≈4-fold larger ΔI values were generated using DMBs compared with magnetic beads labeled with HRP-conjugated anti-*Pf*HRP2 IgG only. These results indicate that the immobilization of additional HRP molecules on the DMBs amplifies the amperometric signal during the electrochemical reaction.

Influence of Blood Dilution on Immunosensor Performance

The use of whole blood for high sensitivity protein detection is challenging due to sample matrix effects. Whole blood is one of the most complex biological matrices since it contains a multitude of cellular and biomolecular components, which can cause interference in immunoassays and diminish the analytical performance.[37] The high viscosity of whole blood can also alter the protein binding efficiency[38] and variations in blood viscosity and ionic composition (pH) among different individuals[39,40] can lead to inconsistent results. Therefore, immunoassays generally involve sample preparation procedures to remove interfering components from blood to reduce matrix effects. Centrifugation is frequently used to separate serum or plasma from whole blood to reduce sample matrix effects and enhance the assay sensitivity. However, centrifugation is labor intensive and requires the use of bulky machinery. To circumvent the need for centrifugation, we investigated whether blood matrix effects could be reduced by simply diluting the sample. Measurements of whole blood with varying dilution factors (0×, 2×, 5× and 20×) spiked with *Pf*HRP2 at 0 ng mL^{-1} and 1 ng mL^{-1} were performed to investigate the effect of blood dilution on the performance of the immunosensor. As shown in Figure 2A, samples with higher dilution factors generated larger values of ΔI. Specifically, the 2× and 5× diluted blood samples generated ≈2-fold and ≈5-fold larger ΔI values, respectively, than those generated from the undiluted blood sample, indicating that sample dilution can significantly diminish blood matrix effects. Diluting whole blood beyond 5× did not result in a noticeable improvement in the sensor performance. These results demonstrate that a 5× dilution factor effectively reduces blood matrix effects for this immunosensor.

We also studied the influence of blood dilution on the reliability of the immunosensor by performing measurements of spiked blood samples, with varying dilution factors, obtained from five independent donors. ΔI values generated from the donor samples with different dilution factors are plotted in Figure 2B (amperometric signals generated from the positive and negative controls from which the ΔI values were determined are presented in Figure S6). The undiluted and 2× diluted blood samples exhibited very large variations in ΔI values, which we attribute to the differences in blood (e.g., viscosity, ionic composition) among the different

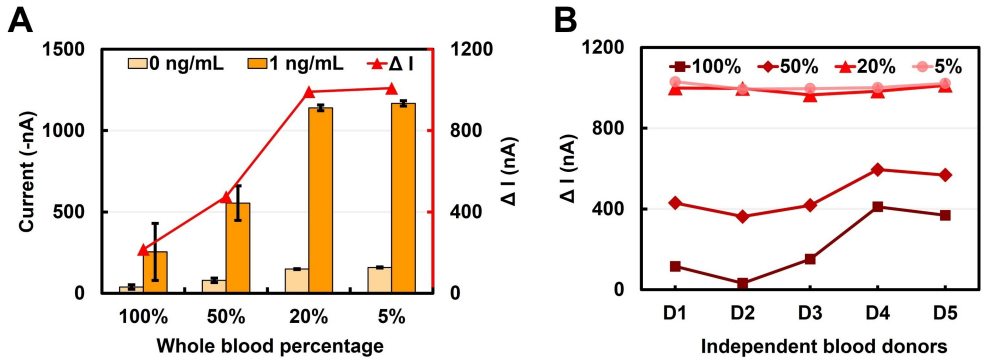

Figure 2. Influence of blood dilution on the sensor performance. A) Amperometric currents generated from whole blood spiked with *Pf*HRP2 at 0 ng mL^{-1} and 1 ng mL^{-1} and corresponding ΔI values with different sample dilution factors (0×, 2×, 5×, and 20×). Each bar represents the mean ± SD of five replicate measurements using new sensors. B) ΔI values generated from whole blood spiked with *Pf*HRP2 at 0 ng mL^{-1} and 1 ng mL^{-1} obtained from five independent blood donor with different sample dilution factors (0×, 2×, 5×, and 20×).

donors. These variations can affect both the ACEF mixing efficiency and protein binding kinetics, which can subsequently alter the response of the sensor. In contrast, the 5× and 20× diluted blood samples generated consistent ΔI values for all five donor samples with a coefficient of variation of <2%. While 20× diluted blood generated ΔI values that were marginally more consistent that those generated by 5× diluted blood, excessive sample dilution can lower the concentration of the target analyte below the LOD of the sensor, effectively diminishing the sensitivity of the assay. Therefore, a 5× dilution factor ensures that this immunosensor generates consistent results when testing blood samples from different individuals while maintaining a high analytical sensitivity.

AC Electrothermal Flow Characterization and Optimization

Numerical simulations were performed to study the characteristics of electrothermally induced flow using a three-electrode configuration and investigate the influence of the sample volume on the electrothermal flow properties. As shown in Figure 3A, the blood sample forms a droplet on the sensor surface and the shape of the droplet is guided by the sample volume. When an AC potential is applied to the sensor, swirling microflows are generated within the droplet between the WE and CE. The simulation results show that the electrothermal flow velocity is influenced by the sample volume, where larger droplets exhibit faster flow velocities. Experimental studies were carried out to measure the amperometric signals generated from blood samples, with varying volumes, spiked with *Pf*HRP2 at 0 ng mL^{-1} and 1 ng mL^{-1}. As shown in Figure 3B, the ΔI values generated from the 80 µL droplet were ≈40 % larger compared with those generated from the 60 µL droplet, demonstrating that faster electrothermal flow can lead to improved sensor performance. However, the ΔI values generated from the 100 µL droplet were ≈12 % lower than those generated from the 80 µL droplet. We hypothesize that excessively fast electrothermal flow causes the surface-immobilized proteins in StabilBlock stabilizer, which is a commercial blocking agent and immunoassay stabilizer that was applied to the sensor, to become detached from the sensor surface, leading to an increase in nonspecific binding, as indicated by the ≈2× higher background signals that were generated for the 100 µL droplet compared with the 80 µL and 60 µL droplets. These results are consistent with prior numerical and experimental studies which show that large fluid forces can cause the detachment of proteins bound to a ligand-coated surface.[41–43]

To visualize electrothermally induced fluid motion, red microbeads were used as tracer particles and added to a 1× PBS droplet on a SPGE sensor that was stimulated by an AC signal. As shown in Figure 3C and Movie S1, the beads are immediately pulled into the swirling flows within 5 s of being dispensed onto the droplet. Within 20 s, the beads move throughout the entire droplet following the streamlines of the flow. The motion of the beads is consistent with the velocity fields predicted by the numerical simulations (Figure 3A). The rapid swirling motion generated by AC electrothermal flow leads to vigorous mixing, which enhances mass transport within the droplet and promotes antigen-antibody reactions. Without ACEF mixing, the motion of the beads is largely directed by buoyancy and diffusion, which causes them to disperse on the surface of the droplet shortly after being dispensed onto the droplet. After ≈20 s, the beads exhibit minimal movement within the droplet (Figure 3C and Movie S2). These results also reveal that particles several microns in diameter can be transported across relatively large distances using AC electrothermal flow, validating its effectiveness for transporting smaller particles, such as proteins and magnetic nanobeads (DMBs). While the electrothermally driven flows generated in this work were limited to buffer and blood samples, we expect that electrothermal flows can also be generated in other biological fluids, such as saliva and urine, further expanding the utility of this method for the development of other types of rapid diagnostic assays.

The ACEF mixing parameters were optimized by performing measurements of blood spiked with *Pf*HRP2 at 0 ng mL^{-1} and 1 ng mL^{-1} using varying potentials (20 V_{pp}, 25 V_{pp} and 30 V_{pp}) and durations (1 min, 3 min, 5 min, 7 min,

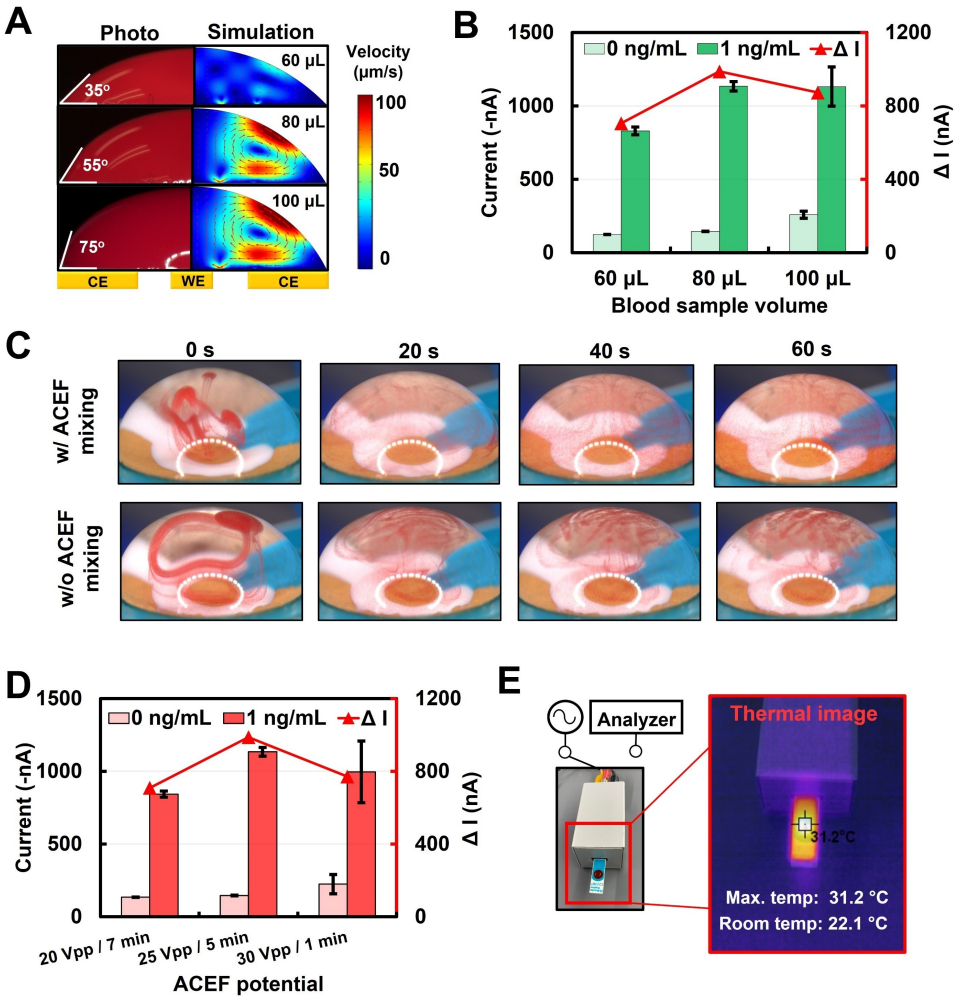

Figure 3. Characterization of ACEF mixing. A) Optical images of 60 μL, 80 μL and 100 μL blood droplets on the SPGE sensor and corresponding 2D COMSOL simulation results of the velocity profile with ACEF mixing (25 V_{pp}, 200 kHz, 5 min). B) Amperometric currents generated from 5× diluted whole blood spiked with *Pf*HRP2 at 0 ng mL^{-1} and 1 ng mL^{-1} and corresponding Δ*I* values with different sample volumes. C) Sequential still frame images showing the motion of 6 μm red polystyrene beads in an 80 μL droplet of 1% BSA in 1× PBS with and without ACEF mixing. D) Amperometric currents generated from 5× diluted whole blood spiked with *Pf*HRP2 at 0 ng mL^{-1} and 1 ng mL^{-1} and corresponding Δ*I* values for different ACEF potentials and mixing durations. Each bar represents the mean ± SD of three replicate measurements obtained using new sensors. E) Experimental setup for performing ACEF mixing and thermal image of an 80 μL blood sample on the SPGE sensor after 5 min of ACEF mixing (25 V_{pp}, 200 kHz).

9 min and 11 min). Prior studies have shown that AC frequencies >100 kHz are necessary for generating electrothermally induced flow[22,44] and that frequencies between 200 kHz and 15 MHz result in similar ACEF performance.[21,45] Therefore, 200 kHz was selected for this work. Amperometric signals and ΔI values for all the tested parameters are presented in Figure S7 and the data for the highest performing parameters are plotted in Figure 3D. The largest Δ*I* values were generated by applying 25 V_{pp} for 5 min, which were ≈40% larger than those generated by applying 20 V_{pp} for 7 min. These results demonstrate that higher AC potentials can lead to an improvement in the sensor performance, even with a shorter mixing duration. However, there was a drop in Δ*I* (and rise in the background signal) when using 30 V_{pp} for 1 min. Since higher AC potentials generate faster electrothermal flows in the droplet, this can cause the surface-immobilized blocking proteins to become detached from the sensor surface, leading to an increase in nonspecific binding as noted above. We also briefly studied the amount of Joule heating produced during ACEF mixing by measuring the temperature of blood droplets using a thermal imaging camera. As shown in Figure S8, the droplet temperature is proportional to the AC potential where larger potentials resulted in higher droplet temperatures. Using the optimized ACEF mixing parameters (25 V_{pp}, 200 kHz, 5 min), we measured a maximum droplet temperature of 31.2 °C (Figure 3E), which is within normal physiological conditions and should not negatively affect the integrity or binding kinetics of proteins in the blood sample.

Performance of the ACEF-Enhanced Magneto-Immunosensor

We first evaluated the improvement in the sensor performance by incorporating ACEF mixing with our electrochemical magneto-immunosensor. Measurements of blood spiked with *Pf*HRP2 at 0 ng mL^{-1} and 1 ng mL^{-1} were performed using the magneto-immunosensor with or without ACEF mixing. The assay parameters for the magneto-immunosensor were optimized and the results are presented in the Supporting Information. Measurements were also performed with ACEF mixing only (without magnetic concentration) and with 1 h of sample incubation (without ACEF mixing or magnetic concentration). The amperometric signals and ΔI values generated with the different sensor enhancement methods is presented in Figure 4A. Measurements performed with 5 min of ACEF mixing (without magnetic concentration) resulted in a ≈7-fold increase in the ΔI values compared with those generated with 1 h of incubation; however, the magnitude of the amperometric signals generated by both methods was extremely low (10's of nA). A significant improvement in the sensor performance was attained using magnetic concentration only, which generated ΔI values that were ≈30-fold larger than those generated with ACEF mixing only. Combining ACEF mixing with magnetic concentration resulted in the largest ΔI values, which were ≈50-fold larger than those generated with ACEF mixing only and 1.5-fold larger than those generated with magnetic concentration only.

We assessed the analytical sensitivity (lower LOD) of the ACEF-enhanced magneto-immunosensor by performing

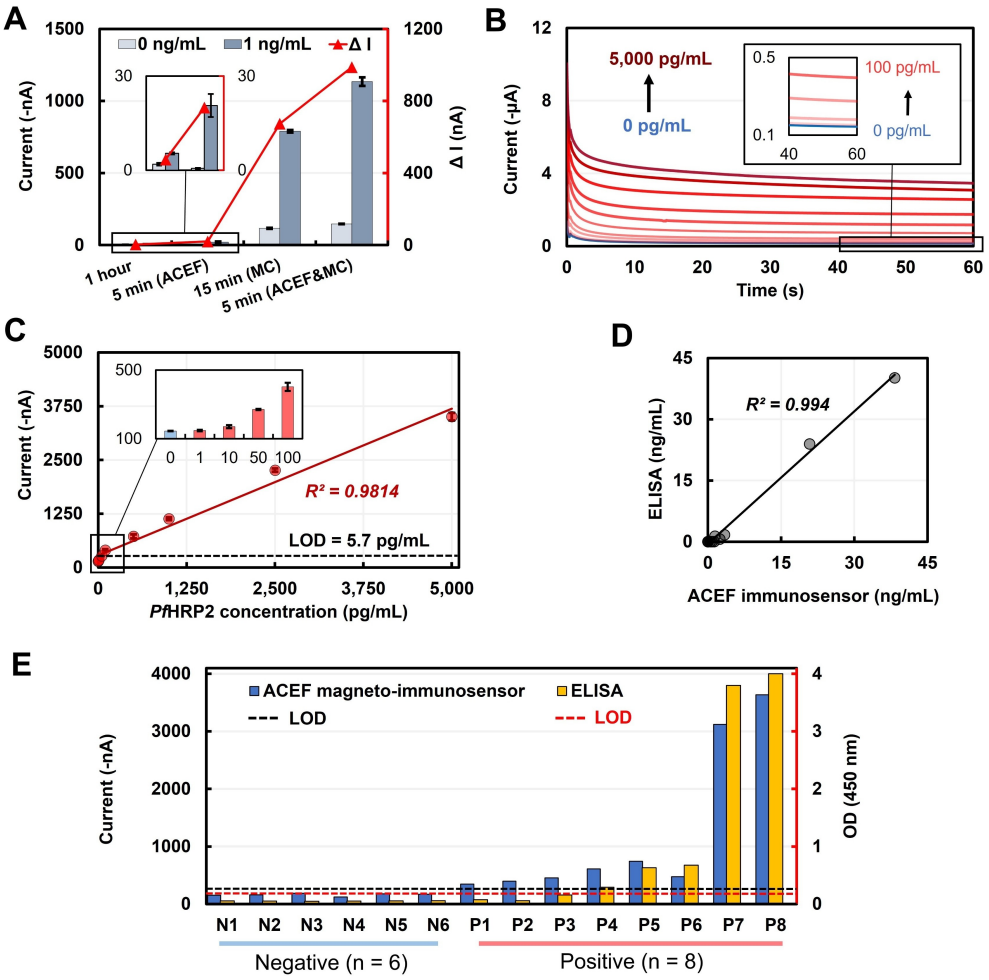

Figure 4. Performance of the ACEF-enhanced magneto-immunosensor for quantifying *Pf*HRP2 in spiked and clinical blood samples. A) Amperometric currents generated from 5× diluted whole blood spiked with *Pf*HRP2 at 0 ng mL^{-1} and 1 ng mL^{-1} and corresponding ΔI values using different sensor enhancement methods. Each bar represents the mean ± SD of three replicate measurements obtained using new sensors. B) Chronoamperograms generated from 5× diluted whole blood spiked with *Pf*HRP2 at concentrations from 0 to 5000 pg mL^{-1} with ACEF mixing and magnetic concentration. C) Calibration plot based on amperometric currents at 60 s obtained from chronoamperograms in panel B. Inset shows amperometric currents for samples containing *Pf*HRP2 from 0 to 100 pg mL^{-1}. Each bar represents the mean ± SD of three replicate measurements obtained using new sensors. The dashed line corresponds to the lower limit of detection, calculated as 3× the SD of the amperometric current at zero concentration divided by the slope of the calibration curve. D) *Pf*HRP2 levels in clinical blood samples measured by the ACEF-enhanced magneto-immunosensor and a commercial *Pf*HRP2 ELISA kit. E) Amperometric signals generated by the ACEF-enhanced magneto-immunosensor and absorbance values (OD 450 nm) generated by ELISA for paired blood samples obtained from individuals with *P. falciparum* infection ($n=8$) and healthy, uninfected individuals ($n=6$).

measurements of blood spiked with increasing concentrations of *Pf*HRP2. Chronoamperograms generated from the blood samples are presented in Figure 4B, which shows a positive correlation between the amperometric current and the *Pf*HRP2 concentration. The calibration curve is presented in Figure 4C, which shows that this immunosensor exhibits a linear response from 0 to 5000 pg mL^{-1} with a R^2 correlation coefficient of 0.9814. The lower LOD of this immunosensor is 5.7 pg mL^{-1}, which was calculated as 3× the standard deviation (SD) of the amperometric current at zero concentration divided by the slope of the calibration curve.[46] This detection limit is several orders of magnitude lower than that of commercially available ELISA tests using whole blood samples.[47–49] In addition, each measurement is completed in 7 min, which is at least 20× faster than conventional ELISA and 7–30× faster than previously reported immunoassays capable of highly sensitive protein detection in whole blood.[12–14]

The selectivity of this immunosensor was evaluated by performing measurements of blood spiked with *Pf*HRP2, pan-*Plasmodium* aldolase or *P. falciparum* lactate dehydrogenase (*Pf*LDH) and non-spiked blood. As shown in Figure S9, the amperometric signals generated from the samples containing *Pf*LDH and aldolase were similar to those generated from the non-spiked blood sample, which was used as a negative control. In contrast, the amperometric signals from the sample containing *Pf*HRP2 were ≈8-fold larger, indicating that this immunosensor is highly selective and will not cross-react with other biomarkers associated with *P. falciparum* infection. The reproducibility of this immunosensor was briefly evaluated by performing measurements of 5× diluted whole blood spiked with *Pf*HRP2 using five batches of sensors and DMBs prepared on different days. As shown in Figure S10, there is a negligible difference (coefficient of variation = 2.7 %) in the ΔI values generated from five different batches of sensors and DMBs, which indicates that this immunosensor offers highly reproducible measurements.

*Pf*HRP2 Quantification in Clinical Blood Samples

To evaluate the accuracy of this immunosensor, we analyzed eight clinical blood samples obtained from malaria patients in Uganda confirmed by microcopy (P1–P8) and six blood samples obtained from healthy, uninfected donors from the U.S. (N1–N6). *Pf*HRP2 measurements were performed on paired blood samples using the immunosensor and a commercial Cellabs Quantimal™ ultra-sensitive *Pf*HRP2 ELISA kit. The *Pf*HRP2 concentration determined by both methods are plotted in a scatter plot (Figure 4D) and linear regression analysis showed that measurements generated by this immunosensor are highly correlated ($R^2 = 0.994$) with those generated by the commercial ELISA kit over a large range of *Pf*HRP2 levels from 0 to 40 ng mL^{-1}. Next, we evaluated the utility of this immunosensor for diagnosing individuals with *P. falciparum* infection based on *Pf*HRP2 measurements in whole blood. Amperometric signals generated by our immunosensor are plotted against the absorbance values generated by the Cellabs ELISA kit for all 14 clinical samples (Figure 4E). A cut-off value of −280 nA was used for discriminating between malaria-positive and malaria-negative cases, which is the amperometric current at the calculated lower LOD of the immunosensor. As shown in Figure 4E, the amperometric signals and absorbance values generated from all six uninfected donor samples (N1–N6) were below the cut-off values for both assays, indicating that both methods were able to accurately identify all the negative cases. When analyzing the malaria-positive samples (P1–P8), the ELISA kit was only able to identify five of the eight samples as positive cases based on the cut-off value specified by the manufacturer. In contrast, the amperometric signals generated from all eight positive samples were above the cut-off value of the immunosensor, indicating that it was able to identify positive cases with better accuracy than the commercial ELISA kit.

Conclusion

In summary, we present an ultrafast biosensor that combines ACEF mixing with an electrochemical magneto-immunoassay for highly sensitive detection of protein biomarkers in whole blood. Through numerical simulations and measurements of *Pf*HRP2 in whole blood, we show that ACEF mixing results in enhanced transport of proteins and DMBs in the sample, which facilitates antigen-antibody interactions and promotes the formation of antigen-DMB immunocomplexes. The synergetic effects of ACEF mixing and immunomagnetic enrichment leads to a larger number of antigen-DMB immunocomplexes attached to the sensor surface within a very short amount of time, giving rise to enhanced amperometric signal generation. Furthermore, by circumventing the need for sample purification and multiple washing and incubation steps, this immunosensor offers improved ease of use compared to conventional immunoassays, making it particularly useful for rapid testing or point-of-care testing. We envision that this platform can be readily adapted to detect other clinically relevant biomarkers by replacing the capture and detection antibodies with different bioreceptors, thereby expanding its utility for rapid disease diagnosis and screening.

Supporting Information

Experimental procedures; discussion of the optimization results for the magneto-immunosensor; figures of the immunosensor performance using varying sample dilution factors, optimization of assay parameters for the ACEF-enhanced magneto-immunosensor, photographs of the SPGE sensor, immunosensor response using sensors coated with and without capture antibody, improvement in signal amplification using DMBs, droplet temperature after ACEF mixing, optimization of the magneto-immunosensor, and selectivity and reproducibility of the immunosensor (PDF).

Movie S1—Video showing the motion of 6 μm polystyrene beads dropped onto an 80 μL droplet of 1 % BSA in 1× PBS with ACEF mixing (25 V_{pp}, 200 kHz) (MP4)

Movie S2—Video showing the motion of 6 μm polystyrene beads dropped onto an 80 μL droplet of 1 % BSA in 1× PBS without ACEF mixing (MP4)

Acknowledgements

We thank Dr. Wen Li for providing assistance with COMSOL simulations. This work was supported in part by the National Institutes of Health (R01AI113257).

Conflict of Interest

The authors declare no conflict of interest.

Data Availability Statement

The data that support the findings of this study are available from the corresponding author upon reasonable request.

Keywords: Blood · Electrochemical · Electrothermal Flow · Immunosensors · Magneto

[1] W. J. Catalona, D. S. Smith, T. L. Ratliff, K. M. Dodds, D. E. Coplen, J. J. J. Yuan, J. A. Petros, G. L. Andriole, *N. Engl. J. Med.* **1991**, *324*, 1156–1161.
[2] A. S. Maisel, J. Koon, P. Krishnaswamy, R. Kazenegra, P. Clopton, N. Gardetto, R. Morrisey, A. Garcia, A. Chiu, A. De Maria, *Am. Heart J.* **2001**, *141*, 367–374.
[3] W. E. Benitz, M. Y. Han, A. Madan, P. Ramachandra, *Pediatrics* **1998**, *102*, e41.
[4] H. Noedl, K. Yingyuen, A. Laoboonchai, M. Fukuda, J. Sirichaisinthop, R. S. Miller, *Am. J. Trop. Med. Hyg.* **2006**, *75*, 1205–1208.
[5] J. D. Doecke, S. M. Laws, N. G. Faux, W. Wilson, S. C. Burnham, C. P. Lam, A. Mondal, J. Bedo, A. I. Bush, B. Brown, K. De Ruyck, K. A. Ellis, C. Fowler, V. B. Gupta, R. Head, S. L. Macaulay, K. Pertile, C. C. Rowe, A. Rembach, M. Rodrigues, R. Rumble, C. Szoeke, K. Taddei, T. Taddei, B. Trounson, D. Ames, C. L. Masters, R. N. Martins, *Arch. Neurol.* **2012**, *69*, 1318–1325.
[6] S. Shrotriya, D. Walsh, N. Bennani-Baiti, S. Thomas, C. Lorton, *PLoS One* **2015**, *10*, e0143080.
[7] J. Kuhle, H. Kropshofer, D. A. Haering, U. Kundu, R. Meinert, C. Barro, F. Dahlke, D. Tomic, D. Leppert, L. Kappos, *Neurology* **2019**, *92*, e1007–e1015.
[8] J. M. Llovet, C. E. A. Peña, C. D. Lathia, M. Shan, G. Meinhardt, J. Bruix, *Clin. Cancer Res.* **2012**, *18*, 2290–2300.
[9] S. K. Vashist, J. H. T. Luong in *Handbook of Immunoassay Technologies* (Eds.: S. K. Vashist, J. H. T. Luong), Elsevier, Amsterdam, **2018**, pp. 1–18.
[10] C. Dincer, R. Bruch, E. Costa-Rama, M. T. Fernández-Abedul, A. Merkoçi, A. Manz, G. A. Urban, F. Güder, *Adv. Mater.* **2019**, *31*, 1806739.
[11] S. D. Gan, K. R. Patel, *J. Invest. Dermatol.* **2013**, *133*, e12.
[12] D. Y. Joh, A. M. Hucknall, Q. Wei, K. A. Mason, M. L. Lund, C. M. Fontes, R. T. Hill, R. Blair, Z. Zimmers, R. K. Achar, D. Tseng, R. Gordan, M. Freemark, A. Ozcan, A. Chilkoti, *Proc. Natl. Acad. Sci. USA* **2017**, *114*, e7054–e7062.
[13] U. Zupančič, P. Jolly, P. Estrela, D. Moschou, D. E. Ingber, *Adv. Funct. Mater.* **2021**, *31*, 2010638.
[14] A. Minopoli, B. Della Ventura, B. Lenyk, F. Gentile, J. A. Tanner, A. Offenhäusser, D. Mayer, R. Velotta, *Nat. Commun.* **2020**, *11*, 6134.
[15] A. Hatch, A. E. Kamholz, K. R. Hawkins, M. S. Munson, E. A. Schilling, B. H. Weigl, P. Yager, *Nat. Biotechnol.* **2001**, *19*, 461–465.
[16] O. Hofmann, G. Voirin, P. Niedermann, A. Manz, *Anal. Chem.* **2002**, *74*, 5243–5250.
[17] I. Pereiro, A. Fomitcheva Khartchenko, R. D. Lovchik, G. V. Kaigala, *Angew. Chem. Int. Ed.* **2021**, *60*, 20935–20942; *Angew. Chem.* **2021**, *133*, 21103–21110.
[18] D. Du, J. Wang, D. Lu, A. Dohnalkova, Y. Lin, *Anal. Chem.* **2011**, *83*, 6580–6585.
[19] I. F. Cheng, H. L. Yang, C. C. Chung, H. C. Chang, *Analyst* **2013**, *138*, 4656–4662.
[20] R. Vaidyanathan, S. Rauf, Y. S. Grewal, L. J. Spadafora, M. J. A. Shiddiky, G. A. Cangelosi, M. Trau, *Anal. Chem.* **2015**, *87*, 11673–11681.
[21] H. Cui, C. Cheng, X. Lin, J. Wu, J. Chen, S. Eda, Q. Yuan, *Sens. Actuators B* **2016**, *226*, 245–253.
[22] Y. Lu, T. Liu, A. C. Lamanda, M. L. Y. Sin, V. Gau, J. C. Liao, P. K. Wong, *J. Lab. Autom.* **2015**, *20*, 611–620.
[23] A. Ramos, H. Morgan, N. G. Green, A. Castellanos, *J. Phys. D* **1998**, *31*, 2338–2353.
[24] Y. Lu, Q. Ren, T. Liu, S. L. Leung, V. Gau, J. C. Liao, C. L. Chan, P. K. Wong, *Int. J. Heat Mass Transfer* **2016**, *98*, 341–349.
[25] M. Sigurdson, D. Wang, C. D. Meinhart, *Lab Chip* **2005**, *5*, 1366–1373.
[26] T. Liu, Y. Lu, V. Gau, J. C. Liao, P. K. Wong, *Ann. Biomed. Eng.* **2014**, *42*, 2314–2321.
[27] W. C. Lee, H. Lee, J. Lim, Y. J. Park, *Appl. Phys. Lett.* **2016**, *109*, 223701.
[28] L. Reverté, B. Prieto-Simón, M. Campàs, *Anal. Chim. Acta* **2016**, *908*, 8–21.
[29] S. Liébana, D. Brandão, S. Alegret, M. I. Pividori, *Anal. Methods* **2014**, *6*, 8858–8873.
[30] J. Min, M. Nothing, B. Coble, H. Zheng, J. Park, H. Im, G. F. Weber, C. M. Castro, F. K. Swirski, R. Weissleder, H. Lee, *ACS Nano* **2018**, *12*, 3378–3384.
[31] B. A. Otieno, C. E. Krause, A. L. Jones, R. B. Kremer, J. F. Rusling, *Anal. Chem.* **2016**, *88*, 9269–9275.
[32] A. Valverde, V. Serafín, J. Garoz, A. Montero-Calle, A. González-Cortés, M. Arenas, J. Camps, R. Barderas, P. Yáñez-Sedeño, S. Campuzano, J. M. Pingarrón, *Sens. Actuators B* **2020**, *314*, 128096.
[33] J. Li, P. B. Lillehoj, *ACS Sens.* **2021**, *6*, 1270–1278.
[34] R. W. Snow, *BMC Med.* **2015**, *13*, 23.
[35] I. Pereiro, A. Fomitcheva-Khartchenko, G. V. Kaigala, *Anal. Chem.* **2020**, *92*, 10187–10195.
[36] J. Grandke, U. Resch-Genger, W. Bremser, L. A. Garbe, R. J. Schneider, *Anal. Methods* **2012**, *4*, 901–905.
[37] C. Selby, *Ann. Clin. Biochem.* **1999**, *36*, 704–721.
[38] M. L. Chiu, W. Lawi, S. T. Snyder, P. K. Wong, J. C. Liao, V. Gau, *JALA J. Assoc. Lab. Autom.* **2010**, *15*, 233–242.
[39] M. Gudmundsson, A. Bjelle, *Angiology* **1993**, *44*, 384–391.
[40] D. D. Van Slyke, *J. Biol. Chem.* **1921**, *48*, 153–176.
[41] J. W. Weisel, H. Shuman, R. I. Litvinov, *Curr. Opin. Struct. Biol.* **2003**, *13*, 227–235.
[42] S. C. Kuo, D. A. Hammer, D. A. Lauffenburger, *Biophys. J.* **1997**, *73*, 517–531.
[43] S. C. Kuo, D. A. Lauffenburger, *Biophys. J.* **1993**, *65*, 2191–2200.

[44] A. Castellanos, A. Ramos, A. González, N. G. Green, H. Morgan, *J. Phys. D* **2003**, *36*, 2584–2597.
[45] M. L. Y. Sin, T. Liu, J. D. Pyne, V. Gau, J. C. Liao, P. K. Wong, *Anal. Chem.* **2012**, *84*, 2702–2707.
[46] D. C. Harris, *Quantitative Chemical Analysis*, W. H. Freeman and Company, New York, **2007**, pp. 84–87.
[47] M. Kawamura, A. Kusano, A. Furuya, N. Hanai, H. Tanigaki, A. Tomita, A. Horiguchi, K. Nagata, T. Itazawa, Y. Adachi, Y. Okabe, T. Miyawaki, H. Kohno, *J. Clin. Lab. Anal.* **2012**, *26*, 174–183.
[48] N. B. Tiscione, K. Wegner, *J. Anal. Toxicol.* **2017**, *41*, 313–317.
[49] C. Klumpp-Thomas, H. Kalish, M. Drew, S. Hunsberger, K. Snead, M. P. Fay, J. Mehalko, A. Shunmugavel, V. Wall, P. Frank, J. P. Denson, M. Hong, G. Gulten, S. Messing, J. Hicks, S. Michael, W. Gillette, M. D. Hall, M. J. Memoli, D. Esposito, K. Sadtler, *Nat. Commun.* **2021**, *12*, 113.

Manuscript received: January 5, 2022
Accepted manuscript online: March 15, 2022
Version of record online: March 30, 2022